ResearchGate

See discussions, stats, and author profiles for this publication at: https://www.researchgate.net/publication/8933890

# Balanol Analogues Probe Specificity Determinants and the Conformational Malleability of the Cyclic 3′,5′-Adenosine Monophosphate-Dependent Protein Kinase Catalytic Subunit

**ARTICLE** *in* BIOCHEMISTRY · FEBRUARY 2004

Impact Factor: 3.02 · DOI: 10.1021/bi035042p · Source: PubMed

CITATIONS
24

READS
22

**7 AUTHORS**, INCLUDING:

Pearl Akamine
Universidad del Caribe (Dominican Republic)
**14** PUBLICATIONS **815** CITATIONS
SEE PROFILE

Nguyen Huu Xuong
University of California, San Diego
**25** PUBLICATIONS **1,782** CITATIONS
SEE PROFILE

Available from: Pearl Akamine
Retrieved on: 30 January 2016

# Balanol Analogues Probe Specificity Determinants and the Conformational Malleability of the Cyclic 3′,5′-Adenosine Monophosphate-Dependent Protein Kinase Catalytic Subunit[†,△]

Pearl Akamine,[‡,§] Madhusudan,[‡] Laurence L. Brunton,[∥] Horng D. Ou,[⊥] Jaume M. Canaves,[▽] Nguyen-huu Xuong,[‡,○] and Susan S. Taylor*[,‡,#]

*Department of Chemistry and Biochemistry, Howard Hughes Medical Institute, and Department of Pharmacology, School of Medicine, University of California, San Diego, La Jolla, California 92093*

*Received June 17, 2003; Revised Manuscript Received October 1, 2003*

ABSTRACT: The protein kinase family is a prime target for therapeutic agents, since unregulated protein kinase activities are linked to myriad diseases. Balanol, a fungal metabolite consisting of four rings, potently inhibits Ser/Thr protein kinases and can be modified to yield potent inhibitors that are selective—characteristics of a desirable pharmaceutical compound. Here, we characterize three balanol analogues that inhibit cyclic 3′,5′-adenosine monophosphate-dependent protein kinase (PKA) more specifically and potently than calcium- and phospholipid-dependent protein kinase (PKC). Correlation of thermostability and inhibition potency suggests that better inhibitors confer enhanced protection against thermal denaturation. Crystal structures of the PKA catalytic (C) subunit complexed to each analogue show the Gly-rich loop stabilized in an "intermediate" conformation, disengaged from important phosphoryl transfer residues. An analogue that perturbs the PKA C-terminal tail has slightly weaker inhibition potency. The malleability of the PKA C subunit is illustrated by active site residues that adopt alternate rotamers depending on the ligand bound. On the basis of sequence homology to PKA, a preliminary model of the PKC active site is described. The balanol analogues serve to test the model and to highlight differences in the active site local environment of PKA and PKC. The PKA C subunit appears to tolerate balanol analogues with D-ring modifications; PKC does not. We attribute this difference in preference to the variable B helix and C-terminal tail. By understanding the details of ligand binding, more specific and potent inhibitors may be designed that differentiate among closely related AGC protein kinase family members.

As cellular processes are better understood at the molecular level, especially in the context of recent genomic information, there has been an increased effort to target specific proteins that are linked to disease. Protein kinases are a diverse family of enzymes that have various regulatory roles yet function similarly by catalyzing the phosphoryl transfer of the $\gamma$-phosphate of ATP[1] to an enzyme-specific protein substrate. Since many diseases, including cancer, autoimmune disorders, cardiac disease, and diabetes, are associated with defects in protein phosphorylation, and there are an estimated ∼500 protein kinases in the human genome (*1*), this family is a major target in the design of pharmaceutical agents and inhibitors. A major challenge for the development of therapeutics is the identification of compounds that have high selectivity. To better understand binding diversity and how this correlates with specificity for protein kinases, three analogues of balanol were studied that specifically inhibit

[†] Portions of this research were carried out at the Stanford Synchrotron Radiation Laboratory, a national user facility operated by Stanford University on behalf of the Office of Basic Energy Sciences, U.S. Department of Energy (DOE). The SSRL Structural Molecular Biology Program is supported by the Office of Biological and Environmental Research, DOE, the Biomedical Technology Program, National Center for Research Resources, National Institutes of Health (NIH), and the National Institute of General Medical Sciences, NIH. This work was funded by NIH Grant GM19301 (S.S.T.) and PHS Grant 5 T32 DK07541 (P.A.). L.L.B. was funded by Grants HL41307 and ES10337.

[△] Atomic coordinates for C:DB1 (access code, 1REJ), C:BD2 (access code, 1RE8), C:BD8 (access code, 1REK) have been deposited in the Protein Data Bank.

* To whom correspondence should be addressed. Phone: (858) 534-3677. E-mail: staylor@ucsd.edu.

[‡] Department of Chemistry and Biochemistry.

[§] Present address: Laboratory of Molecular Biology, Medical Research Council, Cambridge, U.K.

[∥] Department of Pharmacology, School of Medicine.

[⊥] Present address: Biophysics Graduate Group, University of California, San Francisco, CA 94143.

[▽] Present address: Bioinformatics Core, Joint Center for Structural Genomics, San Diego Supercomputer Center, University of California, San Diego.

[○] Department of Physics and Biology, University of California, San Diego.

[#] Howard Hughes Medical Institute.

[1] Abbreviations: cAMP, cyclic 3′,5′-adenosine monophosphate; PKA, cAMP-dependent protein kinase; PKC, calcium- and phospholipid-dependent protein kinase; ATP, adenosine triphosphate; BD, balanol analogue; Bicine, *N*,*N*-bis(2-hydroxylethyl)glycine; Mega-8, octanoyl-*N*-methylglucamide; Mega-9, nonanoyl-*N*-methylglucamide; PKG, cyclic 3′,5′-guanosine monophosphate-dependent protein kinase; CaMKII, calcium calmodulin-dependent kinase II; p34cdc2, cyclin-dependent kinase; BSA, bovine serum albumin; DTT, dithiothreitol; MAPK, mitogen-activated protein kinase; ERK2, extracellular regulated protein kinase-2; IPTG, isopropyl $\beta$-D-thiogalactopyranoside; SSRL, Stanford Synchrotron Radiation Laboratory; Tris−HCl, tris(hydroxymethyl)aminomethane hydrochloride; TFA, trifluoroacetic acid; PDK1, 3-phosphoinositide-dependent kinase-1; PKB, protein kinase B; AGC, PKA, PKG, and PKC.

10.1021/bi035042p CCC: $27.50 © 2004 American Chemical Society
Published on Web 12/09/2003

cyclic 3′,5′-adenosine monophosphate (cAMP)-dependent protein kinase (PKA) over calcium- and phospholipid-dependent protein kinase (PKC).

PKA, one of the simpler, better characterized members of the protein kinase family, serves as a model system. Upon binding the second messenger, cAMP, two C subunits dissociate from the dimeric regulatory subunits. The catalytic core of the C subunit (residues 40−300) is the conserved feature of this family, and conveniently the PKA C subunit activity can be studied independently of the effects of the regulatory domains. In developing inhibitors to protein kinases, the active site of the C subunit—formed by a small lobe (residues 40−120) and a large lobe (residues 128−300)—has been targeted with compounds that compete with ATP binding. The Gly-rich loop (residues 50−55), in the small lobe, is a critical element in ATP binding and phosphoryl transfer (*2*). In the structure of the C subunit complexed with ATP and inhibitor peptide (IP20) (C:ATP:IP20), the enzyme is locked in a stable, closed conformation, by extensive contacts with ATP, where the tip of the Gly-rich loop positions the $\gamma$-phosphate of ATP near catalytic residues in the large lobe.

Because the PKA C subunit has multiple cellular functions, it has not been targeted for the development of disease-related pharmaceutical agents. The PKA regulatory subunit is actively targeted since its overexpression can be isoform specific. For example, the type I regulatory subunit, but not type II, is overexpressed in cancer cells; thus, compounds that bind specifically to the type I regulatory subunit have been sought for cancer therapy (*3*). PKA C subunit specific inhibitors are important as biological tools, to help determine the role of PKA in a given signal transduction pathway.

Balanol, a fungal metabolite, was initially reported as an inhibitor of PKC (*4*−*6*) (Figure 1A). Later, balanol was found to be a competitive inhibitor of ATP and to potently inhibit PKA ($K_i$ = 5 nM), among other Ser/Thr kinases such as PKG, calcium calmodulin-dependent protein kinase II (CaMKII), and p34cdc2 (*7*, *8*). The total synthesis of balanol allowed analogues to be synthesized, which are more specific inhibitors of PKA versus PKC and maintain a high potency for PKA (*7*, *9*). Because of the high homology of the kinase domains (40% identical for PKC residues 340−632 and PKA residues 40−300) (*10*), PKC makes a good companion enzyme to test for inhibitor specificity. These balanol analogues, having an enhanced potency for one protein kinase, provide the opportunity to probe specificity and isoform diversity in the closely related AGC family of protein kinases.

In the previously solved crystal structure of PKA C subunit complexed with balanol (C:Bal), balanol occupied the ATP-binding site (*11*), as predicted by kinetic studies (*7*, *8*) (Figure 1B). Briefly, the *p*-hydroxybenzamide group (A-ring) occupied the adenine ring subsite of ATP, and the hexahydroazepine ring (B-ring) occupied the ribose subsite. The benzophenone group (C- and D-rings) mimicked the triphosphate group of ATP, but occupied a distinct space.

Three analogues of balanol (BD1, BD2, and BD8) that inhibit PKA more potently than PKC are described here (Figure 1A). To examine the molecular basis of protein kinase specificity, three crystal structures of the PKA catalytic (C) subunit complexed to the balanol analogues were solved. Together with biochemical and biophysical

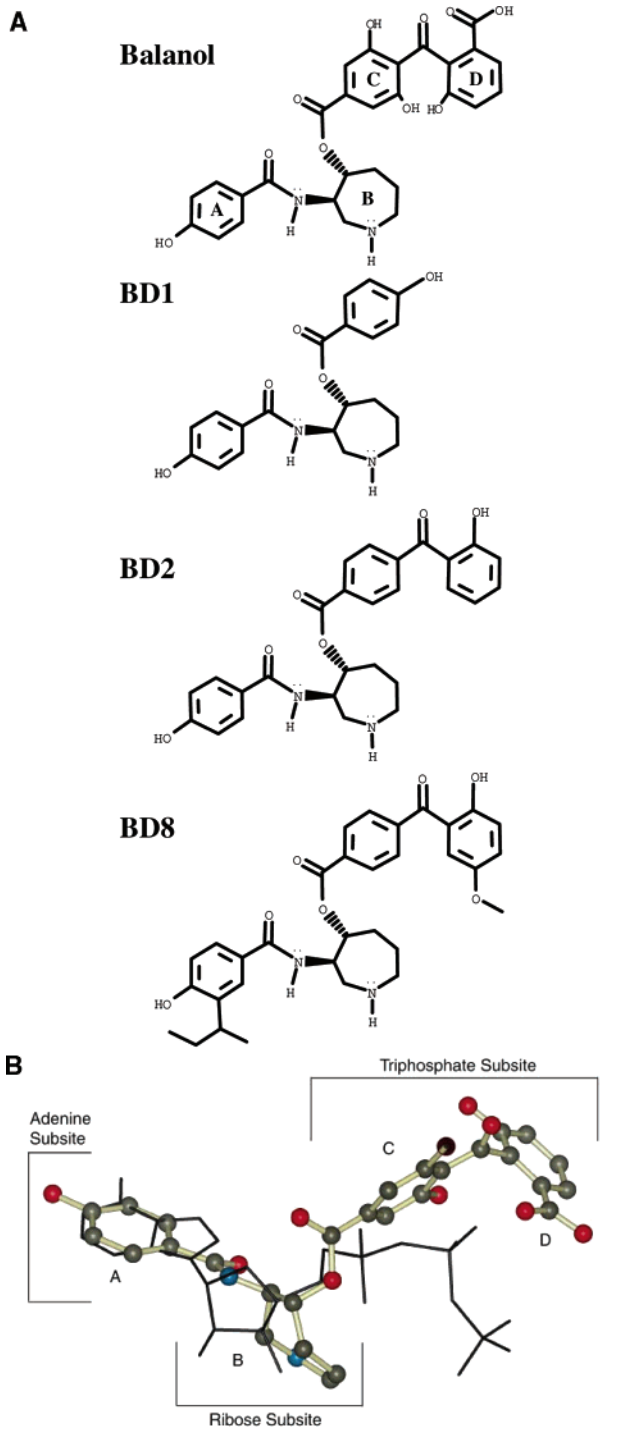


FIGURE 1: Balanol and balanol analogues. (A, top) Chemical diagrams. The most important change is in the D-ring, where the carboxylic acid group in balanol is removed (best seen in BD2). In BD2, the two hydroxyl groups from the C-ring are removed. In comparison to BD2, BD1 has the D-ring removed. BD8 is similar to BD2 but has an additional A-ring alkyl group and an extra *o*-methyl group on the D-ring. This figure was made with the Integrated Scientific Information System (ISIS) Draw program (MDL Information System, Inc., San Leandro, CA). (B, bottom) Balanol and ATP superposition. The A-ring occupies the adenine ring subsite, the B-ring occupies the ribose subsite, and the C- and D-rings mimic the triphosphates, but occupy a distinct space. These spaces are the A-ring subsite, B-ring subsite, and C- and D-ring subsite (*11*). ATP (black stick) was taken from the C:ATP:IP20 structure (PDB code 1ATP) (*2*) and balanol (shown as a ball-and-stick model) from the C:Bal structure (PDB code 1BX6) (*11*). Atoms are colored by type: oxygen (red), nitrogen (blue), and carbon (black).

experiments, the structures provide insight into the specificity of the analogues for PKA, which may aid in the design of other potent and specific PKA C subunit inhibitors. In the absence of a structure of PKC, the analogues serve as probes of the PKC active site local environment.

## EXPERIMENTAL PROCEDURES

*Materials.* Balanol analogues were provided by Dr. Pierre Barbier (Hoffman-La Roche, Basel, Switzerland). Dr. K. C. Nicolaou (University of California, San Diego) provided balanol. PKC $\beta$II was a kind gift from Dr. Alexandra Newton (University of California, San Diego). Reagents were purchased as follows: H1 histone, Mega-8, and Mega-9 (Calbiochem, San Diego, CA); [$\gamma$-$^{32}$P]ATP (ICN Biomedicals, Costa Mesa, CA); NaHEPES (USB, Cleveland, OH); DTT (Roche, Indianapolis, IN); orthophosphoric acid, P81 Whatman paper disks, and dimethyl sulfoxide (DMSO) (Fisher Scientific, Pittsburgh, PA); 2-methyl-2,4-pentanediol (MPD) and ammonium acetate (Aldrich, St. Louis, MO); remaining reagents (Sigma, St. Louis, MO).

*Protein Expression.* Recombinant murine PKA C$\alpha$ was purified as described previously (*12*). Briefly, the C subunit was expressed in BL21 *E. coli* and grown at 37 °C for 6−8 h in LB media prior to induction of protein expression with IPTG. After expression for 6 h at 25 °C, the cells were lysed and the C subunit was purified on a P11 cellulose column. The different phosphorylated species of PKA were separated by cation exchange, using a Mono S column and a salt gradient. Protein from peak II, autophosphorylated on Ser 10, Thr 197, and Ser 338, was used for crystallization and inhibition assays (*12*). For crystallization, purified protein was dialyzed into a 50 mM Bicine buffer with 150 mM ammonium acetate and 10 mM $\beta$-mercaptoethanol, pH 8.0, overnight, then concentrated to 8−10 mg/mL, and sterile filtered. Protein concentration was determined by Bradford assay using BSA standards (*13*).

*Inhibition Assays*. Following a preliminary screen using partially purified PKA and PKC from porcine brain, the analogues were characterized using purified PKA and PKC (*14*).

*(1) PKA Inhibition.* To each reaction was added 5 ng of PKA C$\alpha$. The reaction mixture (100 $\mu$L, final volume) consisted of 30 $\mu$M ATP, 0.3 $\mu$Ci [$\gamma$-$^{32}$P]ATP, 5 mM $MgCl_2$, 1 mM DTT, 0.5 mg mL$^{-1}$ H1 histone, 50 mM NaHEPES (pH 7.5 at 30 °C), and 0.1 mg mL$^{-1}$ BSA (*7*, *8*). Balanol analogue stock solutions were in 10 mM DMSO, while 10× working stocks were prepared with water. The final DMSO concentration, 10% or less, did not affect activity (data not shown). Following incubation for 10 min at 30 °C, 75 $\mu$L aliquots were spotted onto a phosphocellulose paper disk (Whatman P81) and submerged in 500 mL of 0.5% phosphoric acid. The disks were washed batchwise three times more for 5 min each with stirring. The amount of $^{32}$P transferred to H1 histone was quantified by liquid scintillation spectrometry.

*(2) PKC Inhibition.* The activity of PKC was determined using 1 ng of purified rat PKC $\beta$II. The reaction mixture (100 $\mu$L, final volume) consisted of 30 $\mu$M ATP, 0.3 $\mu$Ci [$\gamma$-$^{32}$P]ATP, 5 mM $MgCl_2$, 0.5 mg mL$^{-1}$ H1 histone, 50 mM NaHEPES, pH 7.5 (at 30 °C), 0.5 mM $CaCl_2$, 0.14 mM phosphatidylserine, 4 $\mu$M diacylglycerol, and 0.1 mg mL$^{-1}$ BSA. The experiments were performed as described for PKA (see above).

*(3) Determination of Inhibition Constants.* The inhibition constant, $K_i$, was calculated as previously described (*7*) using the equation $K_i = [(IC_{50})K_d]/(K_d + L)$, where $IC_{50}$ is the concentration of inhibitor that reduced enzyme activity by 50%, $K_d$ is the apparent affinity of the enzyme for ATP, and $L$ is the ATP concentration. The data were plotted using the program Prism (GraphPad, San Diego, CA), assuming a one-site competition. The $K_d$(ATP) values for PKC (7 $\mu$M) and for PKA (19 $\mu$M) were within the range of previously published values (*8*, *15*, *16*). Data were derived from the mean of two to three separate experiments.

*Hydrophobicity Determination of Balanol Analogues*. Reversed-phase HPLC retention time was used to estimate the relative hydrophobicity of balanol and the balanol analogues. Samples of balanol and analogues in 0.1% trifluoroacetic acid (TFA) were applied to an analytical C18 column (Vydac C18, no. 218TP54, 10 $\mu$m particle size, 300 Å pore, 4.6 × 250 mm) and eluted with a linear gradient of 90% acetonitrile in 0.1% TFA. An acidic solvent (TFA) was used to ensure all compounds had the same overall charge so that any interaction with the column could be attributed to the hydrophobic interaction of the compounds with the solid support. A compound with a longer retention time may be interacting more with the column and is presumed to be more hydrophobic.

*Thermostability*. The thermostability of the PKA C subunit (2.5 $\mu$M) in 50 mM potassium phosphate buffer, pH 7.5, was monitored by circular dichroism (CD) using an AVIV 202 CD spectropolarimeter using a 0.1 cm path length microcuvette (40 $\mu$L capacity). C subunit:balanol analogue samples (1:40 ratio) were scanned at 20 °C/h from 30 to 80 °C using a 20 s integration time. The 1:40 C subunit:balanol analogue (BD) ratio used in the thermal unfolding experiments was based on saturation experiments. C subunit:BD ratios assayed were 1:0.25, 1:0.5, 1:1, 1:2, 1:10, 1:20, and 1:40. Simultaneous saturation of the balanol analogue-induced thermal stabilization effect was achieved at the 1:40 ratio, corresponding to a final BD concentration of 100 $\mu$M. Ellipticity was monitored at 222 nm. Each measurement was performed in triplicate. Deviations between scans were negligible. Baseline subtraction and conversion of observed ellipticities (mdeg) to mean residue ellipticities (deg·cm$^2$·dmol$^{-1}$) were performed using the AVIV CDS program. Data analysis, including normalization of maximal and minimal ellipticities to 0−100% folding, was performed using the Microcal Original program, version 3.5. The $T_m$ is the temperature at which 50% of the protein is unfolded.

*Protein Crystallization and Data Collection*. Balanol analogues cocrystallized with the C subunit at 4 °C using the vapor-diffusion hanging-drop method in conditions similar to those of C:Bal (*11*). No metal ions or peptides were used to facilitate crystallization. C:BD1 crystals (0.2 × 0.05 × 0.05 mm) grew in 5 $\mu$L drops with 4.9 mg/mL C subunit, 0.5 mM BD1, 3.3% MPD, and 100 mM Bicine, pH 8.0. The reservoir (1 mL) contained 100 mM Tris−HCl, pH 7.5, and 15% MPD. C:BD2 crystals (0.2 × 0.05 × 0.05 mm) grew in 5.5 $\mu$L drops with 4.5 mg/mL C subunit, 0.45 mM BD2, 3% MPD, 90 mM Bicine, pH 8.0, and 0.1% Mega-9. The reservoir solution (1 mL) contained 100 mM Bicine, pH 8.0, and 15% MPD. C:BD8 crystals (0.6 × 0.2 × 0.05

mm) grew in 3.5 $\mu$L drops with 4.8 mg/mL C subunit, 0.3 mM BD8, 3.3% MPD, 100 mM Bicine, pH 8.0, and 0.3% Mega-8. The reservoir (1 mL) contained 100 mM Tris−HCl, pH 7.5, and 20% MPD. Crystals grew within two to four months. BD1 and BD2 were water soluble. Mega-8 was used to dissolve BD8.

Crystals were cryofrozen at 105 K for C:BD1 and C:BD8 and 96 K for C:BD2 and were cryoprotected with dips in a gradient of increasing MPD/0.1 M Bicine, pH 8.0, starting with 15% and ending with 30% in increments of 5%. A single dip in the final concentration of MPD also provided comparable cryoprotection. C:BD1 and C:BD8 data were collected on the home source, an FR2 rotating anode X-ray generator, which has a Cu K$\alpha$ radiation ($\lambda = 1.54$ Å) that is focused using osmic mirrors, operating at 5 kW. C:BD2 data were collected at SSRL on beam line 7-1. All data were collected from a single crystal using a Mar image plate and were processed using Denzo and Scalepack (*17*). The orthorhombic crystals are isomorphous with other binary crystals—C:adenosine (C:Ade) and C:Bal (*11*, *18*)—with one molecule in the asymmetric unit.

*Structure Solution*. Structures were refined with XPLOR 3.851 (*19*), using C:Bal (PDB code 1BX6) as the starting model (*11*) with balanol omitted and temperature factors (*B* factors) set to a constant value (15−25 Å$^2$). The initial *R* value was 42−44% after rigid body refinement using data to 3 Å. A total of 20−35 rounds of conjugate-gradient positional refinement, slow-cool annealing refinement (with a starting temperature of 2500−3000 K), and individual *B* factor refinement were done, starting with data to 3 Å and in two steps increasing to the highest resolution of the data (*20*). Overall isotropic *B* factor refinement was applied followed by a bulk solvent correction. A $2\sigma_F$ cutoff was used during refinement. Tom/Frodo was used for model building, and analogues were built after the appearance of clear positive $3\sigma_F$ densities in the $F_o - F_c$ map. Residues 1− 15 in C:BD1 and C:BD8 and residues 1−11 in C:BD2 were not seen in the electron density map and are presumed disordered. Totals of 82, 282, and 99 water molecules were built for C:BD1, C:BD2, and C:BD8, respectively, on the basis of a positive $3\sigma_F$ density in the $F_o - F_c$ maps. Only residue 326 of C:BD8 was in the disallowed region of the Ramachandran plot as determined by PROCHECK (*21*, *22*). Figures were made with Insight II (Accelrys Inc., San Diego) or Molscript (*23*).

## RESULTS

*Inhibition Potency*. The balanol analogues inhibit the PKA C subunit with nanomolar potency, but only inhibit PKC with micromolar potency (Figure 2A), and are thus more specific inhibitors than balanol, the parent compound. BD2 has the same basic four-ring structure as balanol, but does not have the two hydroxyl groups on the C-ring or the D-ring carboxylic acid group found in balanol. These modifications significantly enhance the potency of BD2 for PKA ($K_i$ = 0.3 nM versus 5 nM for balanol (*7*)) by over an order of magnitude, while its potency for PKC is decreased by over 2 orders of magnitude (Table 1). The specificity of BD2 for PKA over PKC is thus over 2000-fold. In this regard, BD2 is similar to a previously described balanol analogue that just had the carboxylic acid group removed yet had increased specificity for PKA, but not PKC (*7*, *8*). Thus, the D-ring carboxylic acid group does not appear to contribute to the potency of BD2 for PKA. Since PKC needs the carboxylic acid moiety for balanol binding, a negative charge in this subsite may contribute to PKC ligand binding.

Since BD1 potently ($K_i = 5$ nM) and specifically inhibits PKA, only three of the four rings of balanol are necessary for creating a potent PKA inhibitor. This is surprising since neither the A- and B-rings together nor the C- and D-rings together could inhibit PKA and PKC (*7*). Since only three rings are necessary for creating a potent PKA inhibitor, the synthesis of balanol-based inhibitors can be simplified.

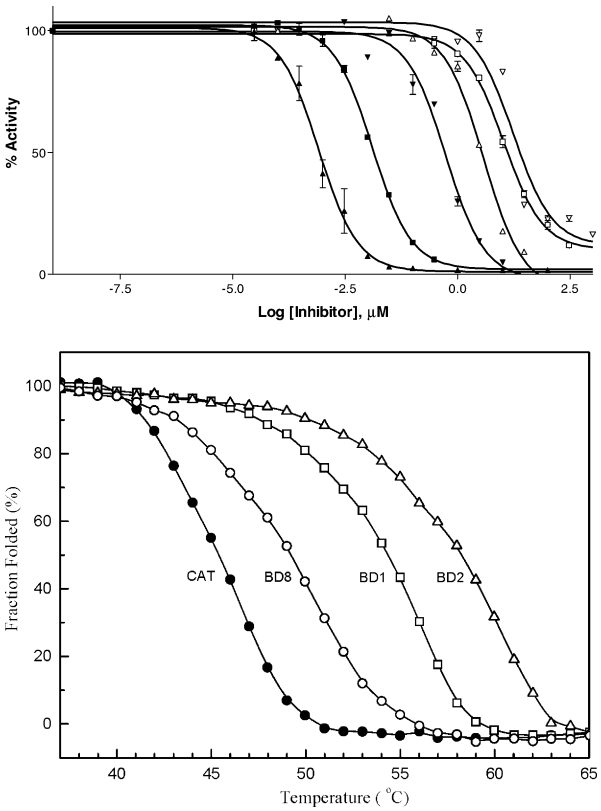


FIGURE 2: Correlation of the inhibition potency and thermostability. (A, top) Inhibition curves for the balanol analogues using PKA and PKC. The $K_i$ for the balanol analogues is in the nanomolar range, whereas the $K_i$ for PKC is in the micromolar range. Filled symbols represent the data for PKA, while the open symbols are for PKC: BD1 data (■), BD2 data (▲), and BD8 data (▼). Table 1 summarizes the $K_i$ values. (B, bottom) Thermostability curves of the balanol analogues as determined by thermal denaturation—monitored by circular dichroism, which measures secondary structure.

Table 1: Biochemical and Biophysical Characteristics of Balanol Analogues[a]

| | $K_i$(PKA) | $K_i$(PKC) | ratio | $H_\phi$ (min) | $T_m$ (°C) |
|---|---|---|---|---|---|
| balanol | 5 | 5 | 1 | 22.1 | na |
| BD1 | 5 | 2000 | 400 | 15.0 | 54 |
| BD2 | 0.3 | 670 | 2200 | 28.7 | 58 |
| BD8 | 200 | 3300 | 17 | 22.1 | 49 |

[a] $K_i$ in nanomolar. For inhibition data $n = 2-3$. The ratio $K_i$ for PKC/$K_i$ for PKA represents the specificity of the compound. $H_f$ is the hydrophobicity measurement as determined by retention time on a C18 column. $T_m$ is the thermostability temperature, with $n = 3$. na means not available.

Table 2: Summary of Balanol Analogue Data and Refinement

| | C:BD1 | C:BD2 | C:BD8 |
|---|---|---|---|
| space group | $P2_12_12_1$ | $P2_12_12_1$ | $P2_12_12_1$ |
| cell dimensions (Å) | $a = 53.5$ | $a = 51.8$ | $a = 53.6$ |
| | $b = 72.1$ | $b = 71.6$ | $b = 71.9$ |
| | $c = 97.6$ | $c = 97.7$ | $c = 98.9$ |
| resolution (Å) | 2.2 | 2.1 | 2.3 |
| completeness (%) | 93 | 95 | 96 |
| $R_{sym}$[a,b] | 6.7 (38) | 8.6 (28) | 7 (19) |
| $R_{refinement}$ | 20.8 | 19.7 | 21.8 |
| $R_{free}$[c] | 29.1 | 25.2 | 29.5 |
| average $B$ (Å$^2$) | | | |
| main chain | 29.7 | 22.4 | 40.1 |
| Gly-rich loop | 27 | 20 | 33 |
| RMSD | | | |
| bond (Å) | 0.01 | 0.01 | 0.01 |
| angle (deg) | 2.9 | 2.6 | 2.5 |
| most favored region (%)[d] | 89.1 | 91.8 | 86.4 |

[a] Values shown in percent. Values in parentheses are for the highest shell. [b] $R_{sym} = \sum|I_{obsd} - I_{av}|/\sum I_{obsd}$. [c] For C:BD1 and C:BD2, 10% of the reflections were in the test set, and for C:BD8, 8% (*44*). [d] Percent of residues in the most favored region of the Ramachandran plot.

BD8 specifically inhibits PKA, but does so with less potency ($K_i = 200$ nM) than BD1 or BD2. While BD8 does resemble BD2, either the A-ring alkyl group or the D-ring *o*-methyl group detrimentally affects BD8 binding to both PKA and PKC, where the consequences are more severe for PKC.

*Hydrophobicity of the Analogues*. On the basis of the order of elution from a C18 column, the compounds in order of decreasing hydrophobicity are BD2, BD8 and balanol, and BD1, where BD2 is the most hydrophobic (Table 1). There is no simple correlation of the relative hydrophobicity of a compound and its inhibition potency. Since balanol successfully inhibited PKA in whole cells (*24*), BD2, which is more hydrophobic and more potent than balanol, should pass through the plasma membrane more readily and thus may be a better inhibitor in intact cells than balanol.

*Balanol Analogues Enhance PKA Thermostability*. Since the thermostability of the C subunit is significantly enhanced when ATP is bound (*25*), the effect of the balanol analogues was also tested. Like ATP, each analogue confers enhanced thermostability to the C subunit—54, 58, and 49 °C for BD1, BD2, and BD8, respectively (Figure 2B), in comparison to 45.4 °C for the unliganded C subunit (Apo). Relative to the thermostability conferred by MgATP ($T_m = 51$ °C) (*25*), the $T_m$ for BD2 is significantly elevated. The increased $T_m$ conveyed by the analogues correlates directly with the increased inhibition potency (Table 1).

*Structure of the C Subunit Bound to BD2: Common Features*. To gain insight into the molecular basis for specificity of the analogues, the crystal structures of the PKA C subunit bound to BD1 (C:BD1), BD2 (C:BD2), and BD8 (C:BD8) were solved (Table 2). Since the three structures

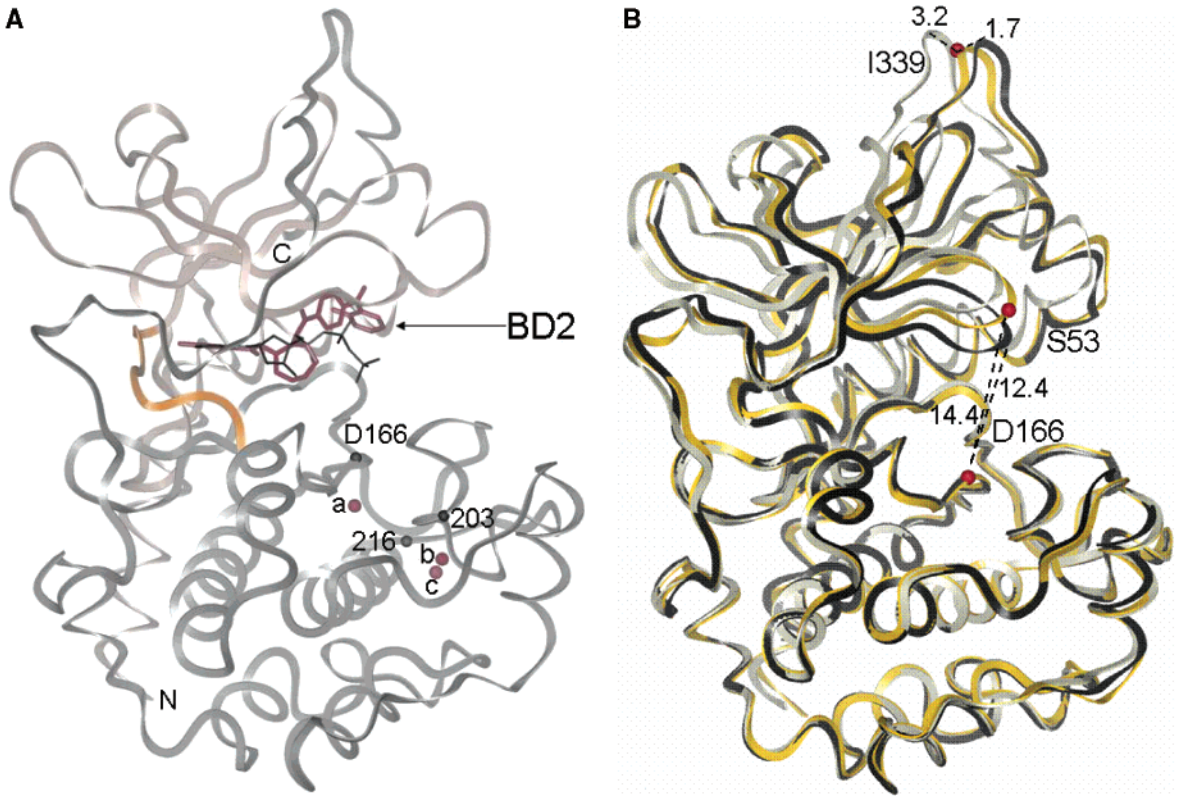


FIGURE 3: The C:BD2 structure is a representative model of the three structures of the C subunit bound to the balanol analogues. (A, left) PKA C subunit complexed with BD2 (red stick model) in the ATP binding site—ATP (black stick model) from C:ATP:IP20 (*2*) after residues 128−300 were superimposed with C:BD2. The ribbon diagram of the C subunit with the N-terminal lobe is shown in beige and the C-terminal lobe in gray. The linker is yellow. Red spheres are three buried water molecules from C:BD2: 405 (a), 389 (b), 374 (c). The water molecules are below the active site and around important catalytic residues. The highly conserved Asp 166 and the two residues that interact with the waters—203 and 216—are shown as black spheres (Cα atoms). N- and C-termini are labeled N and C, respectively. (B, right) C:BD2 adopts an intermediate conformation. The superposition of C:BD2 (yellow) with a closed conformation structure, C:ATP:IP20 (black) (*2*), and C:Bal, an intermediate conformation structure (gray) (*10*) is shown. Ligands are not shown. The Gly-rich loop, represented by Ser 53 Cα (red), is displaced from Asp 166 Cα (red), in the large lobe. Distances (Å) from the three structures are shown for the Cα of Ile 339 (red sphere) as representative of small-lobe displacement.

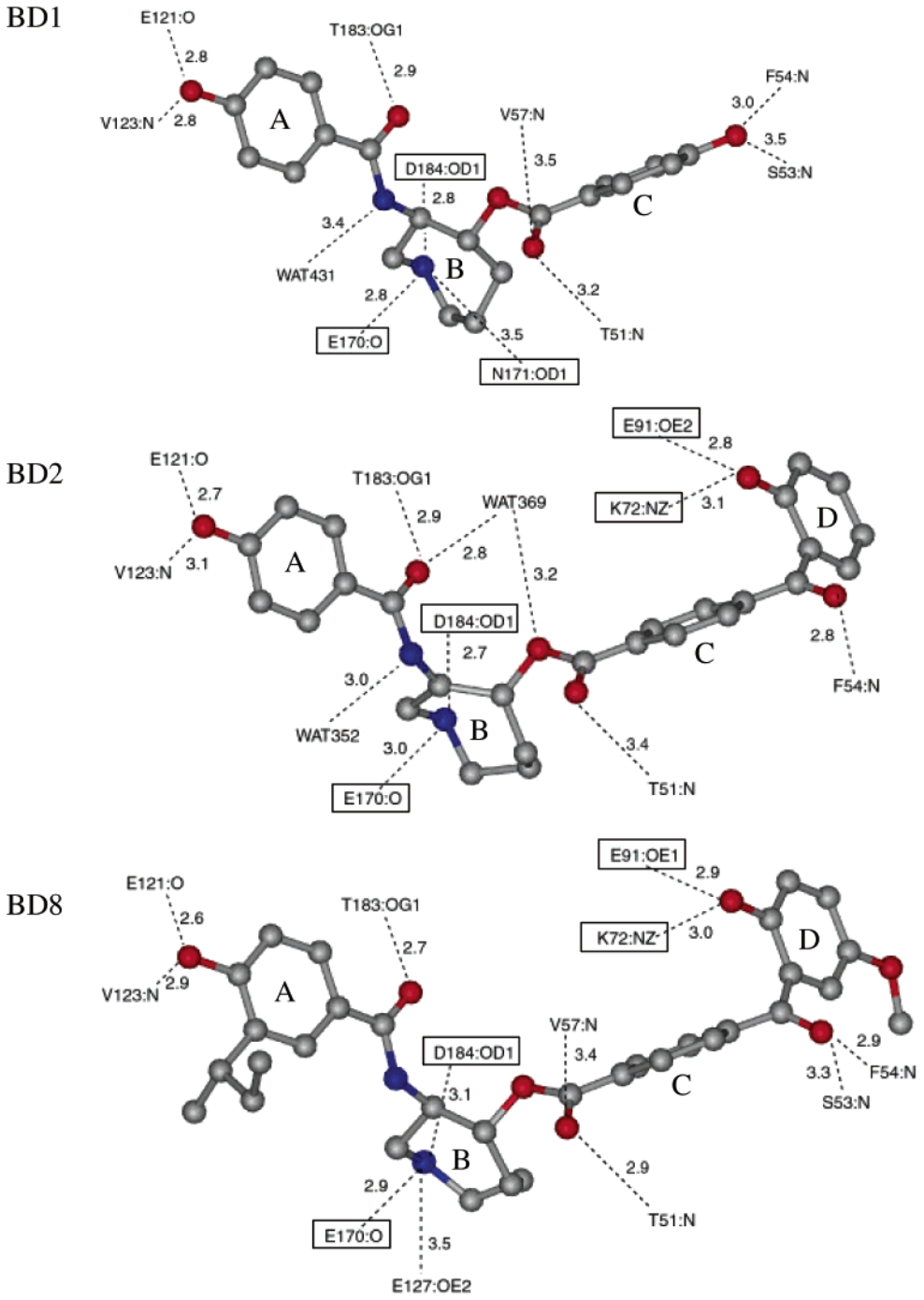


FIGURE 4: Potential hydrogen-bonding interactions for balanol analogues. Potential hydrogen bonds are represented by dashed lines—determined on the basis of polar atoms that are 2.5−3.5 Å apart. Boxes indicate conserved residues. Atoms are colored by type (as in Figure 1). Hydrophobic residues that contribute to ligand binding are listed in Table 3.

are roughly the same (RMSD 0.4 Å), the shared structural features will be highlighted with C:BD2. The three analogues bind to the ATP-binding site (Figure 3A), like all protein kinase small-molecule inhibitors solved to date. In terms of "open" and "closed" conformational states, the C subunit adopts an "intermediate" conformation when the analogues bind. This is slightly more closed than the intermediate conformation of C:Bal (Figure 3B) and is due to the removal of the C-ring hydroxyl groups and the D-ring carboxylic acid group (discussed below). Another indication of a smaller active site is that C:Bal Thr51:N interacts with the ester linkage of balanol via a water molecule, whereas in the C subunit bound to the analogues, this interaction is direct.

Several important hydrogen-bonding interactions are seen in the three structures (Figure 4), as determined by distance measurements. The A-ring hydroxyl of each analogue makes two hydrogen bonds with the backbone of the linker (residues 121−127)—to Glu 121:O and Val 123:N. This interaction, present in most other protein kinase:inhibitor complexes, is not essential for PKA ligand binding, but is for PKC binding (*7*). The B-ring nitrogen hydrogen bonds to Glu 170:O and Asp 184:OD1. The compounds all hydrogen bond to Phe54:N at the tip of the Gly-rich loop (described below).

When the analogues bind the PKA C subunit, numerous polar and nonpolar interactions (Figure 4 and Table 3) disengage the Gly-rich loop in the small lobe from the highly

Table 3. Summary of Hydrophobic Interactions with Balanol Analogues[a]

| balanol subsite | BD1 | BD2 | BD8 |
|---|---|---|---|
| A-ring | V57 | V57 | V57 |
| | A70 | A70 | A70 |
| | | | V104 |
| | M120 | M120 | M120 |
| | | | Y122 |
| | L173 | L173 | L173 |
| | T183 | T183 | T183 |
| | F327 | F327 | |
| B-ring | V57 | V57 | V57 |
| | E127 | E127 | E127 |
| | E170 | E170 | |
| | D184 | D184 | |
| C-ring | G52 | G52 | G52 |
| | K72 | K72 | K72 |
| | L74 | L74 | L74 |
| D-ring | | F54 | F54 |
| | | K72 | K72 |
| | | L74 | L74 |
| | | E91 | E91 |
| | | G186 | G186 |
| | | | F187 |

[a] Letters represent one-letter amino acid names for PKA residues. Hydrophobic interactions are determined by carbon atoms that are within 4 Å of the analogue.

conserved Asp 166, a residue in the large lobe that facilitates catalysis. In the closed conformation, represented by C:ATP:IP20, the Gly-rich loop clamps onto ATP, orients the phosphoryl group during phosphoryl transfer, and positions the phosphoryl group close to residues important for phosphoryl transfer surrounding Asp 166. In C:BD2, the tip of the Gly-rich loop (Ser 53 Cα) is 2 Å further away from Asp 166 Cα than it is in the closed conformation (Figure 3B). The analogues thus wreck the network of interactions at the cleft interface that are important for successful phosphoryl transfer.

*B* factors, indicators of intrinsic atomic disorder, further suggest that the bound analogues rigidify the Gly-rich loop. The average main-chain *B* factor of the Gly-rich loop is lower than the average main-chain *B* factor for the entire C subunit. This is in contrast to C:Ade (*18*) and Apo (*26*) structures, which both have a higher average main-chain *B* factor for the Gly-rich loop (80 and 100 Å$^2$, respectively) than the overall main-chain average (40 and 70 Å$^2$, respectively). The stability of the Gly-rich loop is explained structurally by extensive contacts made with the analogues, not present in C:Ade and Apo. In particular, each analogue can make a key hydrogen bond with Phe54:N, thus stabilizing the tip of the Gly-rich loop. Comparable stability is only seen in closed conformation structures (*2*, *27*, *28*). The Gly-rich loop stabilization may be the structural basis for the enhanced thermostability conferred by the analogues (described above).

Three water molecules are buried in the large lobe of the structures solved (Figure 3A). These waters, clustered around water 405 in C:BD2, were previously unrecognized, but are present in all higher resolution (~2 Å) PKA C subunit structures. Because the waters are within hydrogen-bonding distance to backbone atoms and side chains buried within the hydrophobic core of the protein, they may help maintain the structure. Their proximity to Asp 166, as well as other evidence, suggests that the waters play a role in catalysis. A pool of water, including these three water molecules, is

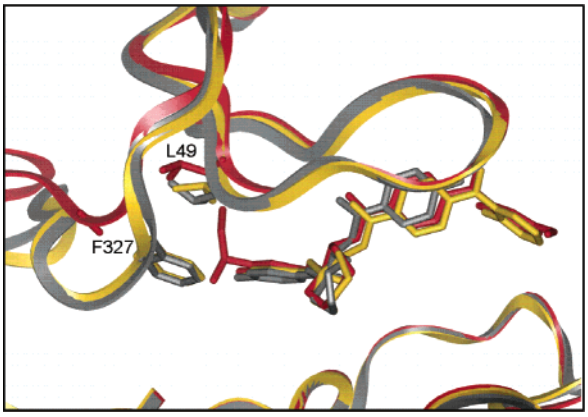


FIGURE 5: Superposition of C:BD1, C:BD2, and C:BD8 structures. The superposition of three structures of the C subunit complexed with each of the balanol analogues, BD1 (gray), BD2 (yellow), and BD8 (red), is shown. The overall structures are similar, but upon BD8 binding the C-terminal tail is perturbed by the alkyl group of the A-ring. Leu 49 and Phe 327 from C:BD8 are displayed.

barricaded by Tyr 204. Mutagenesis of Tyr 204 to Ala detrimentally affects catalysis (*29*) with few structural consequences other than an enlarged pool of water (Yang, J., personal communication), suggesting that the pool of water affects catalysis (*30*).

*Perturbation of the C-Terminal Tail Decreases Inhibitor Potency*. A portion of the "gate" (residues 317−329) of the C-terminal tail (Figure 5) is significantly displaced by the protruding alkyl moiety from the A-ring when BD8 binds the C subunit. Superposition of C:BD8 and the two other analogue-bound structures shows that to accommodate the A-ring of BD8, Phe 327 in the C-terminal tail must move significantly and Leu 49 at the base of the Gly-rich loop is slightly disturbed. These structural differences may explain the reduced potency of BD8. On the other hand, since BD8 does inhibit PKA with nanomolar potency, the C:BD8 structure also illustrates the flexibility of the C-terminal tail, which adjusts to its ligand. A similar disturbance to the C-terminal tail was found when staurosporine, another potent PKA inhibitor, was bound to the C subunit (*31*).

*Active Site Residues Adopt Different Rotamers in the Absence of a D-Ring*. Surprisingly C:BD1 has a structure similar to those of C:BD2 and C:BD8. Even though BD1 has only three rings, to fill the space of the absent D-ring, the active site residues adopt alternate rotamers. For example, Gln 84 points outward from the active site in C:BD2, but points inward when BD1 is bound (Figure 6). Additionally, in C:BD1 Phe 54 is slightly closer to the active site. BD1 shows that the D-ring is necessary for binding PKC, but not for PKA. This is consistent with the Phe 54 to Gly mutant of PKA that bound balanol, suggesting that the Phe 54 to D-ring interaction was not critical (*8*). While Ser 53 and Phe 54 are not essential for balanol binding, interactions that rigidify the Gly-rich loop do appear to be important (*32*).

## DISCUSSION

The fungus *Verticillium balanoides* has likely evolved to synthesize balanol as part of its defense system, since the inhibition of protein kinases such as PKA and PKC would stop cell growth and function. In the search for specific protein kinase inhibitors, balanol is an appealing starting compound because it is a highly potent, broad-based Ser/Thr protein kinase inhibitor. Furthermore, since balanol can

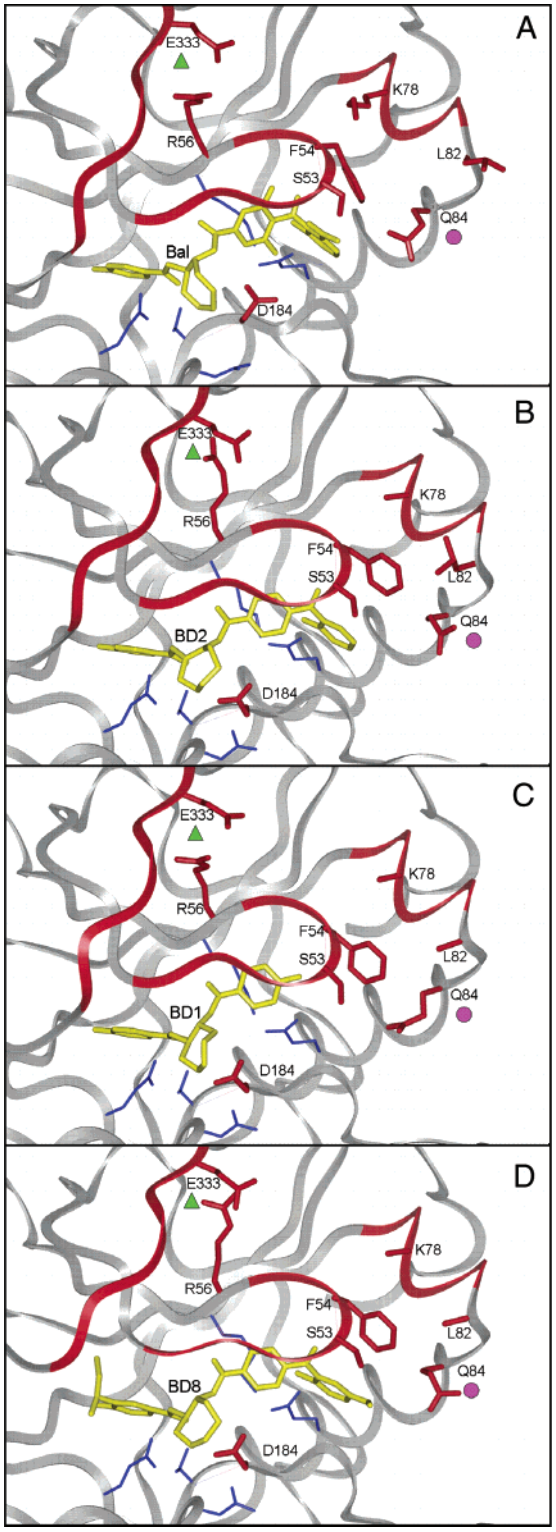


FIGURE 6: Local conformational changes upon ligand binding. Close-up of variable regions of the C subunit: C:Bal (A), C:BD2 (B), C:BD1 (C), and C:BD8 (D). Side chains (red) of active site residues adopt different rotamers depending on the ligand bound. Alternate rotamers are utilized to optimize hydrophobic and hydrophilic interactions. Shown are Lys 78 and Leu 82 from the B helix, Gln 84 from the C helix, Ser 53, Phe 54, and Arg 56 from the Gly-rich loop, Glu 333 from the C-terminal tail, and Asp 184 from the large lobe. Gln 84 (pink circle) adopts alternate rotamers depending on the ligand bound. The Arg 56 to Glu 333 salt bridge (green triangle) is lost when the inhibitors bind. In blue are residues that do not change conformation. Inhibitors are in yellow. The Gly-rich loop and the variable B helix and C-terminal tail, which interact with the Gly-rich loop, are red ribbons.

be chemically synthesized, it can be modified to create specific inhibitors. Being cell permeable (*24*), balanol is suitable for the development as an inhibitor for application in vivo. Although achieving specificity may be complicated, in the design of effective therapeutics, one encouraging success story is Gleevec (STI-571), an anticancer agent that specifically inhibits the hyperactive Abelson tyrosine protein kinase, which is responsible for myelogenous leukemia (*33*).

Here, the analysis of balanol analogues that retain their potency for PKA, but not PKC, provides a window to highlight key differences between the two enzymes. The manner in which the analogues interact with each enzyme allows the identification of specific subsites within the active site that may be targeted in the combinatorial design of PKA inhibitors derived from balanol. From this study we hope to determine general rules about the molecular mechanism of ligand binding and specificity, which would provide a paradigm for understanding how inhibitor specificity can be achieved for a closely related enzyme subfamily, such as the AGC protein kinase family.

In terms of open and closed conformational states, these structures show that a potent inhibitor does not have to mimic a transition state. The balanol analogues appear to stabilize the Gly-rich loop in an intermediate conformation. Thus, in the case of the protein kinases, where the small lobe is quite malleable, inhibitors have a wide array of conformations to sample. Furthermore, since the $K_i$ of the analogues correlated with $T_m$, thermostability may be used to screen for inhibitor potency, where compounds that confer a higher $T_m$ to the C subunit are better inhibitors.

How do the four rings of balanol contribute to the inhibition of PKA activity and to specificity? A hydrophobic group that occupies the A-ring subsite appears to be a common requirement of all ATP-based kinase inhibitors (*11*, *31*, *33*, *34*). Typically, the A-ring moiety also hydrogen bonds to the backbone of the linker, but this is not essential (*7*). This is consistent with previous computational work that showed that the potency of balanol was due to the nonpolar interactions, but specificity was determined by the electrostatic contribution from polar groups (*35*). Additional substituents to the balanol A-ring that disturb the C-terminal tail (as in C:BD8) appear to detrimentally affect binding to both PKA and PKC; however, the effect is less severe in PKA.

A positive charge at the nitrogen position of the B-ring has been highlighted as an important feature in ligand binding. An interaction with this charged group is preserved in the structures of C:Bal and the analogues (*11*, *35*). The conformational flexibility of the seven-membered ring allows sufficient freedom for the nitrogen to be within hydrogen-bonding distance to the carbonyl oxygen of Glu 170. Computational analysis showed that this nitrogen enhances ligand binding thermodynamically (*36*). The absence of a C-ring hydroxyl group in the analogues allows Asp 184 to hydrogen bond to the B-ring nitrogen, by adopting a different rotamer than the one found in C:Bal. This is another example of an active site residue adjusting to accommodate a functional group of a ligand.

Unlike PKA, PKC can tolerate changes in the B-ring subsite (*37*, *38*). Three residues that contact adenosine in the C:ATP:IP20 structure differ in PKA and PKC; Leu 173, Thr 183, and Glu 127 in PKA are Met, Ala, and Asp in

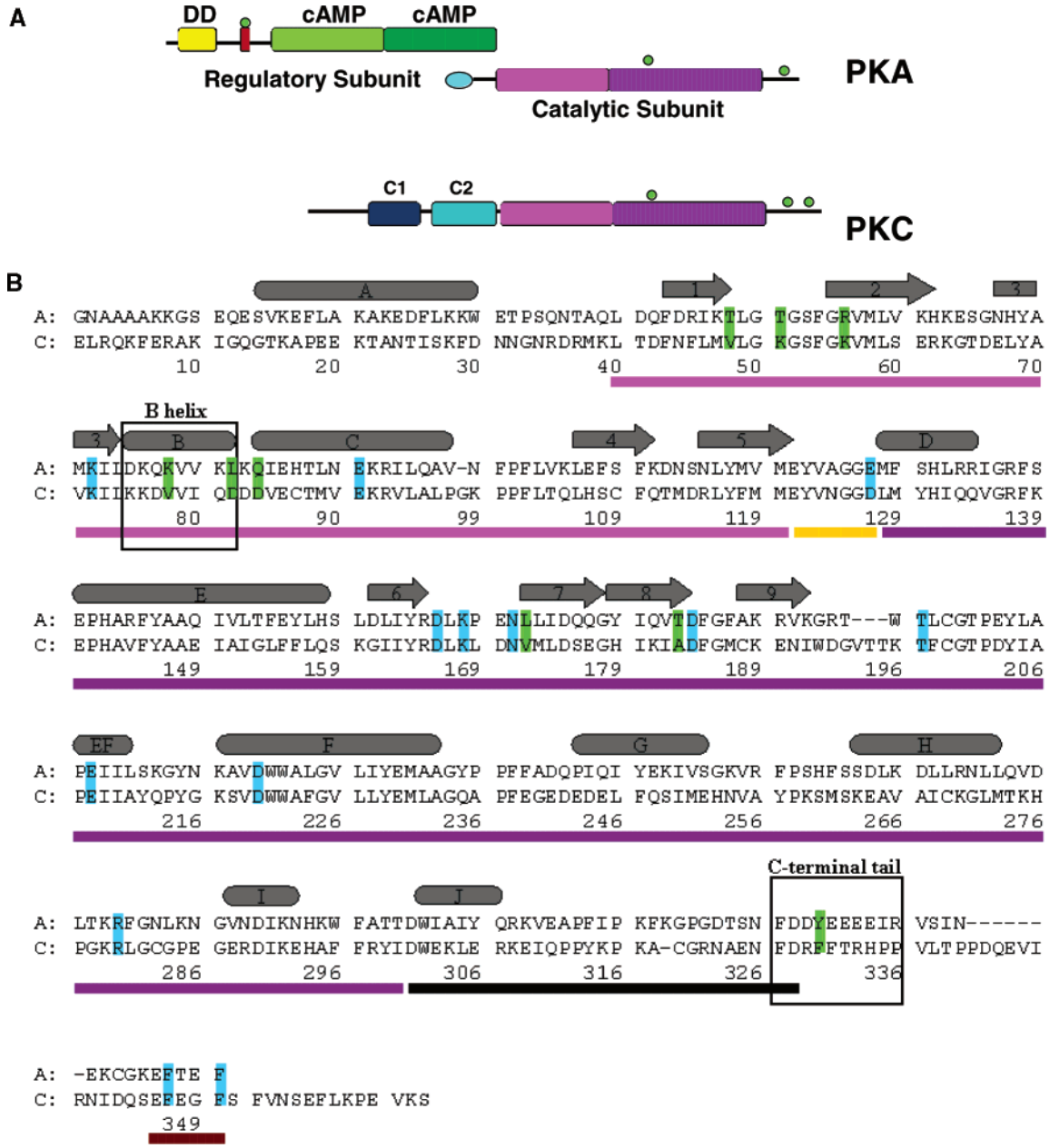


FIGURE 7: PKA versus PKC. (A, top) PKA and PKC shared kinase core. Pink and purple bars represent the small (residues 40−120) and large (residues 128−300) lobes, respectively. The PKA C subunit and R subunit (two green bars represent the cAMP-binding domains) are in different polypeptide chains, in contrast to PKC that has its regulatory domains, C1 (blue) and C2 (light blue) domains that bind $Ca^{2+}$ and phospholipids, in the same polypeptide. Yellow indicates the dimerization/docking domain, red indicates the autoinhibitory site, and green balls are sites of phosphorylation. The light blue sphere is a myristylation site. (B, bottom) Sequence alignment of PKA Cα and PKC βII kinase domains. Green boxes are variable residues that approach the ligand-binding site. Black boxes are the variable regions between PKA and PKC that may play a role in the difference in inhibition potency. Blue boxes are conserved residues. Gray ovals and arrows represent α helices and β strands. Pink and purple bars demarcate the small and large lobes, with the linker in yellow. C-terminal regions that are similar in PKA and PKC are in black and brown bars for the large- and small-lobe anchors.

PKC, respectively (Figures 7B and 8B). Together these residues provide a larger cavity in PKC around the B-ring subsite (Figure 8C); this would allow PKC to accommodate bulkier, bicyclic and tricyclic groups (*37*, *38*) that PKA could not.

C:BD1 highlights that the A-, B-, and C-rings are necessary for creating a PKA-specific inhibitor based on balanol, but the D-ring is not. Furthermore, the analogues demonstrate that PKA, in contrast to PKC, is tolerant of alterations in the D-ring subsite.

One reason that balanol inhibits PKA and PKC whereas the analogues inhibit only PKA may be that balanol props the active site cleft open slightly more than the analogues do (Figure 3B). PKC has an additional C1 domain that binds diacylglycerol and phorbol esters and a C2 domain that binds acidic phospholipids and $Ca^{2+}$ (Figure 7A), but how these regulatory domains interact with the kinase domain is not known. If the C1 and C2 domains interact with the kinase domain favorably when balanol is bound, those favorable interactions may be lost when the analogues bind and the active site cleft is slightly more closed.

The slightly more open active site cleft in C:Bal is likely due to the direct interaction of the balanol C-ring hydroxyl group with the Gly-rich loop (Gly 52 and Gly 55 backbone

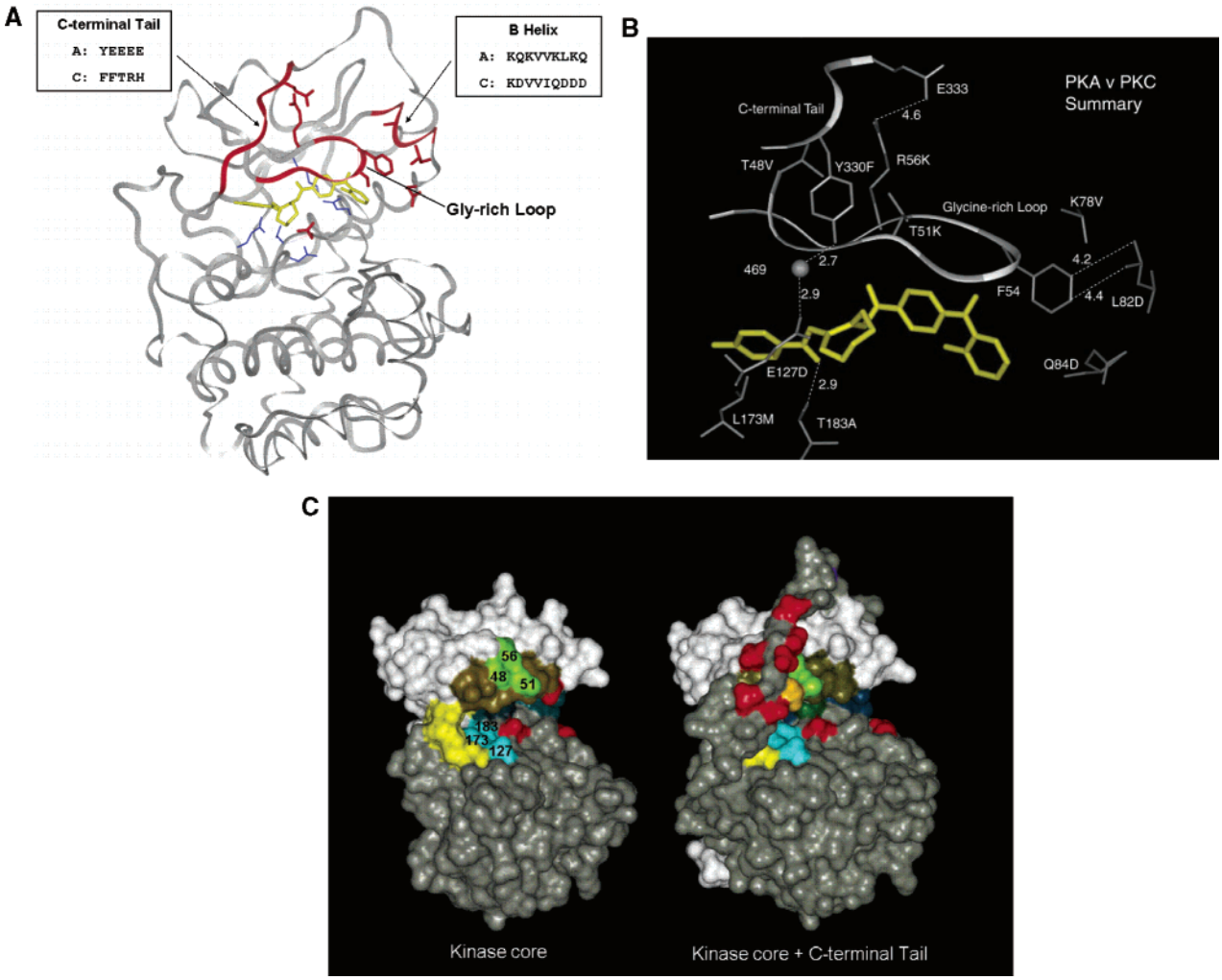


FIGURE 8: Variable regions between PKA and PKC. (A, top left) Overview of C:BD2. Proximal to the conserved Gly-rich loop (residues 50−55, red), the B helix (residues 76−80, red) and the C-terminal tail (residues 330−334, red) are variable between the two protein kinases and may account for the difference in inhibition potency of the analogues. In PKA, a stretch of Glu residues in the C-terminal tail is not present in PKC. In PKC, a stretch of Asp residues in the B helix is not present in PKA. Residues that may contribute to interaction with the D-ring are Lys 78, Leu 82, and Gln 84 (B and C helices), Ser 53 and Phe 54 (Gly-rich loop), and Glu 333 (C-terminal tail), which interacts with Arg 56 in the ternary complex with C:ATP:IP20 (*2*) (not shown). (B, top right) Close-up of the active site. The variable regions can be divided into three areas: the A- and B-ring subsites (Glu 127, Leu 173, and Thr 183), the C-terminal tail, and the B helix. The cumulative effect of amino acid changes in the A- and B-ring subsites for PKC is an enlarged binding pocket. One-letter amino acid names are used. The first letter and number are the amino acid in PKA, and the second letter is the equivalent PKC amino acid. Dashed lines are potential hydrogen-bonding or salt bridge interactions. A water (gray sphere) that contacts Tyr 330 coordinates several regions of the protein—the C-terminal tail, Glu 127, which interacts with the ribose moiety of ATP, and the P-3 Arg from IP20 (*45*). BD2 is yellow. (C, bottom) Highlight of the surface covered by the C-terminal tail. The kinase core alone (left) and kinase core plus C-terminal tail (right) show how the C-terminal tail is an integral part of the active site and creates the gate region that allows entrance to the active site. The 1ATP structure is shown (*2*). White and gray indicate the small and large lobes with the linker in yellow. Green residues are from the base of the Gly-rich loop, which are different in PKA and PKC. In blue are residues that differ around the A- and B-ring subsites. Asp 184, Ser 53, and Thr 197 are in red on the left, and acidic residues from the C-terminal tail are in red on the right. Tyr 330 is displayed in orange.

atoms), which is absent with the analogues. The steric hindrance or the electron repulsion of the C-ring hydroxyl groups and the D-ring hydroxyl group and carboxylic acid group may contribute to this interaction by orienting the C- and D-rings appropriately. The charge present on the carboxylic acid group of balanol may also contribute to the balanol interaction with PKC, which is not present in the analogues.

The main chemical difference between balanol and the analogues is the carboxylic acid group in the D-ring. In C:Bal, this carboxylic acid group is within hydrogen-bonding distance to Ser 53 (hydroxyl group) (*11*); however, since Ser 53 is conserved between PKA and PKC, this interaction alone cannot account for the difference in potency. To examine residues in the proximity of Ser 53, a sequence homology alignment (*10*) and the C subunit structure were used to create a preliminary model of the PKC active site (Figures 7 and 8). Although residues directly surrounding the D-ring—Lys 72, Glu 91, and Phe 54 (hydrogen-bonding residues) (Figure 4) and Leu 74 and Gly 186 (hydrophobic contact residues)—are all conserved between PKA and PKC, there are two variable segments surrounding the Gly-rich loop that may account for the binding specificity of the balanol analogues—helix B and the C-terminal tail (Figure 8A).

*The Variable B Helix*. The B helix structure is conserved among the PKA, PDK1, and PKB structures (*39*, *40*), all members of the AGC family; therefore, the B helix is likely

to be structurally conserved in PKC. While the position of the B helix backbone is likely the same, the electrostatic and hydrophobic properties are not. Specifically, several polar residues in the PKC B helix are hydrophobic in PKA and vice versa; Lys 78 is a Val, Leu 82 is an Asp, and Gln 84 is an Asp in PKA and PKC, respectively. These residues lie just above the tip of the Gly-rich loop (Figure 8B) and introduce an acidic patch in PKC that is absent in PKA. In PKC, the charge repulsion between the D-ring carboxylic acid group and the B helix may be necessary to open the cleft sufficiently to accommodate the D-ring of balanol.

*The Variable C-Terminal Tail.* While the kinase core is conserved in all protein kinases, the N- and C-terminal regions are highly variable and interact with the core in different ways. In Src, the SH2−kinase domain linker interacts with the loop between the C helix and $\beta$ strand 4 (*41*), whereas in PKA the N-terminal A helix covers this region. In MAPK ERK2, although the N-terminal tail has a very different sequence and structure, it interacts with the kinase core surface in a manner similar to that of the PKA C-terminal tail FXXF motif (residues 347−350). Additionally, the ERK2 C-terminal tail wraps around the large lobe and covers an area of the kinase core similar to the area covered by the PKA N-terminal A helix. In the case of PKC, we can only speculate as to how the C-terminal tail or the C1 and C2 domains interact with the kinase core. On the basis of sequence similarities of PKA, PDK1, and PKC, the C-terminal tail of PKC is predicted to interact with the large lobe of the kinase domain on the same surface as PKA initially (residues 301−314—the large lobe anchor) (*18*). At the PKC C-terminus, the FXXF motif should firmly anchor the C-terminal tail onto the docking motif created by the C helix on the surface of the small lobe as seen in PKA (*39*).

The region that covers the active site in PKA is a "gate" (residues 315−334) that changes conformation to allow access to the active site (*18*, *26*). An acidic patch (residues 328−334) within the gate is thought to be a "latch", since it interacts with the Gly-rich loop. Because PKC has seven additional residues in this segment of the C-terminal tail, the PKC C-terminus probably covers more area of the kinase core than the PKA C-terminus. Furthermore, since the PKC C-terminal tail does not have an acidic patch, it probably covers a different surface of the kinase core than the PKA C-terminal tail. These two differences between the PKA and PKC C-terminal tails may affect the shape of the active site and therefore ligand specificity.

Molecular dynamics simulations suggest that a salt bridge, from Glu 333 in the latch to Arg 56 in the Gly-rich loop, plays a role in the closing of the Gly-rich loop (*42*). To support this idea, when PKA is in the closed conformation (in C:ATP:IP20), Glu 333 and Arg 56 are within salt-bridging distance (*2*), and when the C subunit binds the balanol analogues, this ion pair is broken (Figure 8B). If the Gly-rich loop is the lid of the active site, then Arg 56 may be a handle that is pushed down upon by the C-terminal tail. In PKC, however, this Arg is a Lys and the acidic patch is absent in the C-terminal tail. Additionally, Thr 48, which interacts with Arg 56 in PKA, is a Val in PKC. In the absence of the contacts found in PKA, the PKC C-terminal tail and Gly-rich loop interactions are predicted to be different (Figure 8C) and may operate in a different way. For example, in PKC, an acidic patch from helix B, rather than from the C-terminal tail, may play a role in determining the path of the C-terminal tail across the kinase core surface and in closing the Gly-rich loop, which has yet to be shown.

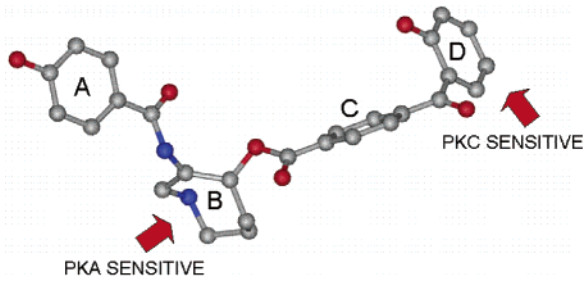


FIGURE 9: Balanol analogues as a probe for designing specific inhibitors. BD2 is shown as a model for how analogues derived from balanol may be designed. In PKA, the D-ring subsite is tolerant of modification, but not in PKC. In PKC, the B-ring subsite can accommodate large bulky substituents; however, PKA cannot.

In ligand binding, the PKA C-terminal tail is important for excluding solvent from the active site—especially Phe 327, which creates a hydrophobic environment around the A-ring subsite (*43*). The PKA latch of the C-terminal tail may play a role in the Gly-rich loop movement, and the PKC C-terminal tail may play a similar role. As an integral part of the active site, the PKA C-terminal tail may be targeted in drug design since it varies among protein kinases (*36*).

*Balanol Analogues as Probes.* This work shows that PKA is slightly sensitive to changes in the A-ring subsite but tolerates changes in the D-ring subsite. PKC, on the other hand, cannot tolerate changes in the D-ring subsite. It is likely that the PKC C-terminal tail interacts more with the D-ring subsite than is seen with the PKA C-terminal tail, which would explain why PKC is more sensitive to modifications in this region. In designing a PKA inhibitor, this suggests that the D-ring subsite is a better target for modification. On the other hand, since PKC tolerated large substituents at the B-ring subsite (*37*, *38*), the B-ring appears to be a better target for modification in the development of PKC-specific inhibitors (Figure 9).

In the absence of PKC structural information, sequence alignment and a structural model derived from PKA help to understand some of the differences between PKA and PKC. Furthermore, the balanol analogues provide a mechanism to test the model and to probe the local environment of the active site to help identify determinants for ligand binding.

## ACKNOWLEDGMENT

We offer special thanks to Teresa Clifford and Celina Juliano for providing the purified C subunit, Nick Nguyen for data collection support, Joan Kanter, Michael Moore, and Sharmin Schauble for help with the inhibition assays, Elzbieta Radzio-Andzelm for help in creating the figures, and Nina Haste for help in preparing the manuscript.

## REFERENCES

1. Manning G., Whyte D. B., Martinez R., Hunter T., and Sudarsanam S. (2002) *Science 298*, 1912−1934.
2. Zheng, J., Knighton, D. R., ten Eyck, L. F., Karlsson, R., Xuong, N., Taylor, S. S., and Sowadski, J. M. (1993) *Biochemistry 32*, 2154−2161.
3. Tortora, G., and Ciardiello, F. (2002) *Ann. N. Y. Acad. Sci. 968*, 139−147.

4. Kneifel, H., König, W. A., Loeffler, W., and Müller, R. (1977) *Arch. Microbiol. 113*, 121−130.
5. Kulanthaivel, P., Hallock, Y. F., Boros, C., Hamilton, S. M., Janzen, W. P., Ballas, L. M., Loomis, C. R., Jiang, J. B., Katz, B., Steiner, J. R., and Clardy, J. (1993) *J. Am. Chem. Soc. 115*, 6452−6453.
6. Boros, C., Hamilton, S. M., Katz, B., and Kulanthaivel, P. (1994) *J. Antibiot. 47*, 1010−1016.
7. Koide, K., Bunnage, M. E., Gomez Paloma, L., Kanter, J. R., Taylor, S. S., Brunton, L. L., and Nicolaou, K. C. (1995) *Chem. Biol. 2*, 601−608.
8. Setyawan, J., Koide, K., Diller, T. C., Bunnage, M. E., Taylor, S. S., Nicolaou, K. C., and Brunton, L. L. (1999) *Mol. Pharm. 56*, 370−376.
9. Nicolaou, K. C., Bunnage, M. E., and Koide, K. (1994) *J. Am. Chem. Soc. 116*, 8402−8403.
10. Orr, J. W., and Newton, A. C. (1994) *J. Biol. Chem. 269*, 8383−8387.
11. Narayana, N., Diller, T. C., Koide, K., Bunnage, M. E., Nicolaou, K. C., Brunton, L. L., Xuong, N. H., Ten Eyck, L. F., and Taylor, S. S. (1999) *Biochemistry 38*, 2367−2376.
12. Yonemoto, W., McGlone, M. L., Grant, B., and Taylor, S. S. (1997) *Protein Eng. 10*, 915−925.
13. Bradford, M. M. (1976) *Anal. Biochem. 72*, 248−254.
14. Orr, J. W., Keranen, L. M., and Newton, A. C. (1992) *J. Biol. Chem. 267*, 15263−15266.
15. Bhatnagar, D., Roskoski, R., Jr., Rosendahl, M. S., and Leonard, N. J. (1983) *Biochemistry 22*, 6310−6317.
16. Lew, J., Coruh, N., Tsigelny, I., Garrod, S., and Taylor, S. S. (1997) *J. Biol. Chem. 272*, 1507−1513.
17. Otwinowski, Z., and Minor, W. (1997) *Methods Enzymol. 276*, 307−326.
18. Narayana, N., Cox, S., Nguyen-huu, X., Ten Eyck, L. F., and Taylor, S. S. (1997) *Structure 5*, 921−935.
19. Brunger, A. T., Kuriyan, J., and Karplus, M. (1987) *Science 235*, 458−460.
20. Brunger, A. T., Krukowski, A., and Erickson, J. (1990) *Acta Crystallogr. A46*, 585−593.
21. Ramachandran, G. N., and Sasisekharan, V. (1968) *Adv. Protein Chem. 23*, 283−438.
22. Laskowski, R. A., MacArthur, M. W., Moss, D. S., and Thornton, J. M. (1993) *J. Appl. Crystallogr. 26*, 283−291.
23. Kraulis, P. J. (1991) *J. Appl. Crystallogr. 24*, 946−950.
24. Gustafsson, A. B., and Brunton, L. L. (1999) *Mol. Pharm. 56*, 377−382.
25. Herberg, F. W., Doyle, M. L., Cox, S., and Taylor, S. S. (1999) *Biochemistry 38*, 6352−6360.
26. Akamine, P., Madhusudan, Wu, J., Xuong, N. H., Ten Eyck, L. F., and Taylor, S. S. (2003) *J. Mol. Biol. 327*, 159−171.
27. Bossemeyer, D., Engh, R. A., Kinzel, V., Ponstingl, H., and Huber, R. (1993) *EMBO J. 12*, 849−859.
28. Madhusudan, Akamine, P., Xuong, N. H., and Taylor, S. S. (2002) *Nat. Struct. Biol. 9*, 273−277.
29. Moore, M. J., Adams, J. A., and Taylor, S. S. (2003) *J. Biol. Chem. 278*, 10613−10618.
30. Dwyer, J. J., Gittis, A. G., Karp, D. A., Lattman, E. E., Spencer, D. S., Stites, W. E., and Garcia-Moreno, E. B. (2000) *Biophys. J. 79*, 1610−1620.
31. Prade, L., Engh, R. A., Girod, A., Kinzel, V., Huber, R., and Bossemeyer, D. (1997) *Structure 5*, 1627−1637.
32. Grant, B. D., Hemmer, W., Tsigelny, I., Adams, J. A., and Taylor, S. S. (1998) *Biochemistry 37*, 7708−7715.
33. Schindler, T., Bornmann, W., Pellicena, P., Miller, W. T., Clarkson, B., and Kuriyan, J. (2000) *Science 289*, 1857−1859.
34. Engh, R. A., Andreas, G., Kinzel, V., Huber, R., and Bossemeyer, D. (1996) *J. Biol. Chem. 271*, 26157−26164.
35. Hünenberger, P. H., Helms, V., Narayana, N., Taylor, S. S., and McCammon, J. A. (1999) *Biochemistry 38*, 2358−2366.
36. Wong, C. F., Hunenberger, P. H., Akamine, P., Narayana, N., Diller, T., McCammon, J. A., Taylor, S., and Xuong, N.-H. (2001) *J. Med. Chem. 44*, 1530−1539.
37. Mendoza, J. S., Jagdamm, G. E., and Gosnell, P. A. (1995) *Bioorg. Med. Chem. Lett. 5*, 2211−2216.
38. Lai, Y.-S., Mendoza, J. S., Jagdmann, G. E., Menaldino, D. S., Biggers, C. K., Heerding, J. M., Wilson, J. W., Hall, S. E., Jiang, J. B., Janzen, W. P., and Ballas, L. M. (1997) *J. Med. Chem. 40*, 226−235.
39. Biondi, R. M., Komander, D., Thomas, C. C., Lizcano, J. M., Deak, M., Alessi, D. R., and van Aalten, D. M. (2002) *EMBO J. 21*, 4219−4228.
40. Yang, J., Cron, P., Thompson, V., Good, V. M., Hess, D., Hemmings, B. A., and Barford, D. (2002) *Mol. Cell 9*, 1227−1240.
41. Williams, J. C., Weijland, A., Gonfloni, S., Thompson, A., Courtneidge, S. A., Superti-Furga, G., and Wierenga, R. K. C. A. P. L. (1997) *J. Mol. Biol. 274*, 757−775.
42. Tsigelny, I., Greenberg, J. P., Cox, S., Nichols, W. L., Taylor, S. S., and Ten Eyck, L. F. (1999) *Biopolymers 50*, 513−524.
43. Batkin, M., Schvartz, I., and Shaltiel, S. (2002) *Biochemistry 39*, 5366−5373.
44. Brunger, A. T. (1992) *Nature 355*, 472−474.
45. Shaltiel, S., Cox, S., and Taylor, S. S. (1998) *Proc. Natl. Acad. Sci. U.S.A. 95*, 484−491.

BI035042P